

# COUPLED THERMO-MECHANICAL ANALYSIS AND SHAPE OPTIMIZATION FOR REDUCING UNEVEN WEAR OF BRAKE PADS

Myeong Jae Han<sup>1)</sup>, Chul Hyung Lee<sup>1)</sup>, Tae Won Park<sup>2)\*</sup>, Jung Min Park<sup>3)</sup> and Sung Min Son<sup>4)</sup>

<sup>1)</sup>School of Mechanical Engineering, Ajou University, Gyeonggi 16499, Korea

<sup>2)</sup>Department of Mechanical Engineering, Ajou University, Gyeonggi 16499, Korea

<sup>3)</sup>Extreme Technology R&D Center, Korea Automotive Technology Institute, 303 Pungse-ro, Pungse-myeon, Dongnam-gu, Cheonan-si, Chungnam 31214, Korea

<sup>4)</sup>Automotive Technology Center, E. S. Brake, 65-40 Sangmasingi-ro, Daegot-myeon, Gimpo-si, Gyeonggi 10043, Korea

(Received 10 February 2017; Revised 21 March 2017; Accepted 10 May 2017)

**ABSTRACT**—In vehicle braking systems, the non-uniform contact pressure distribution on the brake pad is a major cause of uneven wear. The experimental approach of the wear phenomenon is the time consuming and costly. For this reason, a three-dimensional finite element (FE) model of a brake system is presented for numerical simulation in this paper. A coupled thermo-mechanical analysis is carried out to confirm the non-uniform contact pressure distribution. A correlation between the non-uniform contact pressure and uneven wear is confirmed by measuring the amount of wear in the brake pad. The shape optimization of the brake pad is performed to reduce the uneven wear. In addition, the simulation results, such as natural frequency and temperature, are compared to experimental results.

**KEY WORDS** : Coupled thermo-mechanical analysis, Contact pressure distribution, Uneven wear, Shape optimization, Brake dynamometer test

## 1. INTRODUCTION

A brake system decelerates a rotating disc by applying pad pressure. At this time, the kinetic energy of the vehicle is converted into thermal energy through frictional contact between the disc and pads (Thomas *et al.*, 2002). Thus, a braking phenomenon is a non-linear problem involving frictional contact and heat generation between two different bodies. In particular, the heat generation while braking causes a material deformation that changes the contact pressure, which is referred to as thermoelastic instability (Lee and Barber, 1994). The system instability of the brake pads divides a contact surface into four zones, depending on the contact characteristics. Each zone may have effects such as stick, slip, and separation conditions, or may exist as a combination of them. These various contact characteristics lead to a change in the contact pressure distribution of the pad (Baillet *et al.*, 2005). A change in contact pressure distribution is the main reason for the uneven wear on the relatively weak material surface (Soderberg and Andersson, 2009).

Numerous studies have been devoted to the brake system. Parker and Marshall (1948) experimentally identified the fact that heat generation between two bodies

under sliding friction produces non-uniform contact pressure. Meziane *et al.* (2007) carried out a theoretical and experimental work on the instability of a disc-pad system. When instability occurs, the various contact surface conditions generate impact forces. These impact forces give rise to periodic shocks in time and frequency. In a numerical study on the contact analysis, Pantuso *et al.* (2000) proposed a formula for contact conditions between two solids based on the FE method for the thermo-mechanical problem. Gao *et al.* (2006) carried out a thermal stress analysis of thermal fatigue by constructing a three-dimensional FE model for a simple disc brake system. Jung *et al.* (2011) implemented a hot judder phenomenon for a specific vibration mode that occurs above the disc critical velocity using a staggered approach numerical analysis technique. The frictional force at the sliding contact surface may significantly affect the pressure distribution and wear process (Soderberg and Andersson, 2009). Simulation results of the wear model show a reasonably good correlation with the experimental results in the static contact pressure and wear height distributions (Abubakar and Ouyang, 2008). Hassan *et al.* (2009) carried out a fully coupled thermo-mechanical analysis to provide the contact and temperature distribution before executing a squeal analysis. Wu *et al.* (2016) performed a thermal fatigue crack growth analysis and life evaluation for a

---

\*Corresponding author. e-mail: park@ajou.ac.kr

railway brake disc using an extended finite element method (XFEM) and virtual node polygonal finite element method (VPM). From many previous studies, it can be concluded that the non-uniform contact pressure distribution is a major cause of uneven wear. However, there is hardly any coupled thermo-mechanical analysis for wear prediction.

In this paper, a three-dimensional FE model of the disc brake system is proposed. The non-uniform contact pressure distribution on the pad surface that occurs during single braking was confirmed using a coupled thermo-mechanical analysis. The wear amount in the brake pad was measured using a brake dynamometer test to confirm the correlation between the non-uniform contact pressure distribution and uneven wear. A shape optimization for the reduction of uneven wear was carried out. An objective function that can predict the non-uniform contact pressure distribution was derived.

## 2. THEORETICAL BACKGROUND

### 2.1. Coupled Thermo-mechanical System Procedure

The frictional contact of two different bodies has heat generation and structural elastic effects, simultaneously. In a sequential approach, system equations in two different domains such as the structural and the thermal models are solved separately. The information obtained from two different domains is exchanged and updated for each iteration time. In addition, the kinetic energy should be calculated from the specification of the vehicle and the braking conditions to input a heat flux. Therefore, the sequential approach does not have the direct coupled effects of the frictional model.

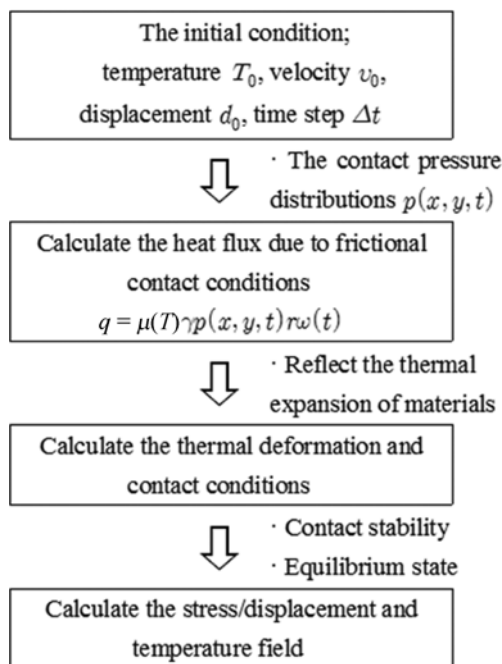


Figure 1. Coupled thermo-mechanical analysis procedure.

In essence, a numerical approach of the coupled thermo-mechanical system proceeds by exchanging information between the structural and the thermal models at every incremental time. The procedure for the coupled thermo-mechanical analysis is presented in Figure 1. In the initial condition, the node displacement and velocity of the structural model and the temperature distribution of the thermal model are in a static equilibrium state. The input pad pressure forms a contact pressure distribution between the disc and the pad. In this case, the heat flux is calculated from the contact pressure, friction coefficient, relative speed, different radius and heat partition ratio. The thermal expansion and contact conditions are obtained from the entering heat flux. Finally, when the convergence condition is satisfied from the appropriate contact conditions, the corrected displacement and temperature distribution results are obtained.

### 2.2. Contact Pressure Distribution and Wear

One of the main roles of the brake caliper is to press the pads as evenly as possible against the rotor. A uniform pressure between the disc and pads results in uniform wear and temperature, and a more stable friction coefficient. However, if a non-uniform contact pressure distribution occurs during braking, then the pad wears unevenly. Depending on the direction of rotation of the disc, the region where the friction begins (leading surface) has a larger wear amount than the region where the friction ends (trailing surface). Moreover, if there is a groove on the friction surface, the contact pressure and wear are concentrated around the groove. This uneven wear is caused by higher pressure at the leading surface than that at the trailing surface (Limpert, 1999). Therefore, the numerical analysis approach is needed to predict the uneven wear, by accurately implementing the non-uniform contact pressure distribution.

### 2.3. Finite Element Formulation

The three-dimensional FE model for a typical brake system is schematically presented in Figure 2. The brake system is

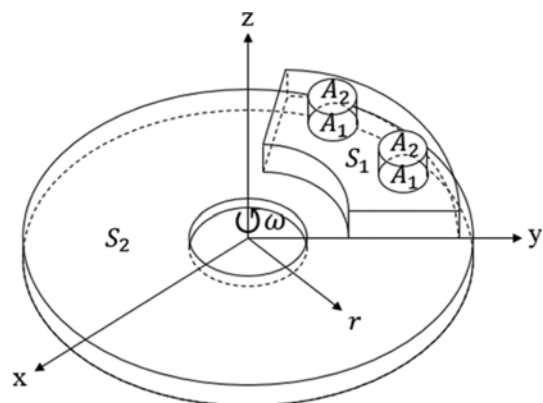


Figure 2. Three-dimensional FE model for brake system.

a multibody system composed of one disc, two pads and four pistons. The surface  $S_1$  of the disc and the pad is partial contact region. The surface  $S_2$  of the disc is the non-contact region (also called the free surface). The surface  $A_1$  of the pad and the piston is the contact region. The surface  $A_2$  of the piston is the region for piston pressure. The brake disc rotates counter-clockwise with an angular velocity  $\omega$ . A different radius of the disc is  $r$ .

2.3.1. Governing equations

The thermal energy caused by friction is dissipated by heat conduction through the contact surface between the disc and pads and by convection from the non-contact surface. To apply the thermal model, it is assumed that: (i) All properties are isotropic and thermal properties are temperature-independent. (ii) The friction coefficient is temperature-dependent. (iii) The brake pressure by the piston is non-uniformly distributed on the contact surface between the disc and pads. (iv) Convective heat transfer by constant ambient temperature rather than external flow is considered. (v) Radiative heat transfer is not considered.

The transient heat conduction equation of the brake system for the three-dimensional problem described in the Cartesian coordinate system is given as follows:

$$\rho c \left( \frac{\partial T}{\partial t} \right) = k \left\{ \frac{\partial}{\partial x} \left( \frac{\partial T}{\partial x} \right) + \frac{\partial}{\partial y} \left( \frac{\partial T}{\partial y} \right) + \frac{\partial}{\partial z} \left( \frac{\partial T}{\partial z} \right) \right\} \quad (1)$$

where  $\rho$ ,  $c$ , and  $k$  are the density, specific heat, and thermal conductivity, respectively. The initial boundary condition for the heat transfer problem can be expressed as follows:

$$T = T_0 \text{ at } t = 0 \quad (2)$$

$$-k \frac{\partial T}{\partial z} = q \text{ on } S_1, \quad 0 < t < t_s \quad (3)$$

$$-k \frac{\partial T}{\partial z} = h(T_{S1} - T_\infty) \text{ on } S_1, \quad 0 < t < t_s \quad (4)$$

$$-k \frac{\partial T}{\partial z} = h(T_{S2} - T_\infty) \text{ on } S_2, \quad 0 < t < t_s \quad (5)$$

where  $T_0$ ,  $T_{S1}$ ,  $T_{S2}$ , and  $T_\infty$  are the initial temperature, surface  $S_1$  temperature, surface  $S_2$  temperature, and ambient temperature, respectively.  $q$  is the heat flux entering in the contact surface.  $h$  is the convection coefficient on the free surface. The boundary surfaces  $S_1$  and  $S_2$  are the heat flux and convective heat transfer field, respectively. Heat transfer occurs only in braking times.

2.3.2. Convection coefficient

To calculate the exact temperature of the disc and the pad, it is necessary to consider the convective heat transfer on the free surface. The convective heat transfer proceeds from the high temperature disc surface to the low temperature ambient air. The convection coefficient can be formulated as follows (Frank *et al.*, 2013):

$$h = Pr^{0.3} k_a \left[ 0.037 \left( \frac{u_\infty L}{\nu} \right)^{0.8} - A \right] / L \quad (6)$$

where  $Pr$  ( $= 0.7$ ) is the Prandtl number,  $k_a$  ( $= 2.63 \times 10^{-2}$  W/m<sup>2</sup>C) is the thermal conductivity of the air,  $u_\infty$  ( $= 4$  m/s) is the free stream velocity for braking speed 100 km/h,  $L$  ( $= 2\pi r$ ) is the characteristic length of the disc,  $\nu$  ( $= 15.89 \times 10^{-6}$  m<sup>2</sup>/s) is the kinematic viscosity and  $A$  is the constant determined from the critical Reynolds number.

$$A = 0.037 Re^{0.8} - 0.0664 Re^{0.5}, \quad \left( Re = \frac{u_\infty L}{\nu} \right) \quad (7)$$

2.3.3. Heat generation caused by frictional contact

In order to simplify the analysis model, it is assumed that the braking pressure is constant and the angular velocity decreases linearly with time during the braking. The angular velocity of the disc is derived as follows:

$$\omega(t) = \omega_0 \left( 1 - \frac{t}{t_s} \right), \quad 0 < t < t_s \quad (8)$$

where  $\omega_0$  is the initial angular velocity and  $t_s$  is the braking time. Heat generation caused by frictional contact between the disc and the pad is calculated as frictional heat flux. In the contact surface  $S_1$ , the heat flux  $q$  can be derived as follows:

$$q = \mu(T) \gamma p(x, y, t) r \omega(t) \quad (9)$$

where  $\mu$  is the friction coefficient,  $\gamma$  is the heat partition ratio,  $p$  is the contact pressure, and  $r$  is the different radius. The heat partition ratio  $\gamma$  can be obtained as follows (Yevtushenko and Grzes, 2011):

$$\gamma = \frac{1}{1 + \sqrt{\rho_p k_p c_p / \rho_d k_d c_d}} \quad (10)$$

where  $k_d$  and  $k_p$  are the conductivity of the disc and the pad,  $\rho_d$  and  $\rho_p$  are the density of the disc and the pad, and  $c_d$  and  $c_p$  are the specific heat of the disc and the pad, respectively. Therefore, the heat flux entering the disc and the pad is determined as follows:

$$q_d = \mu(T) \gamma p(x, y, t) r \omega(t) \quad (11)$$

$$q_p = \mu(T) (1 - \gamma) p(x, y, t) r \omega(t) \quad (12)$$

3. ANALYSIS MODEL

3.1. FE Model Information

The FE model is constructed using an 8-node hexahedron linear element. The total number of elements is 8,020 and the number of nodes is 13,574. In this study, the commercial software ABAQUS Ver. 6.13 was used.

The material properties of each component are shown in Table 1. To consider the thermoelastic effect of frictional contact, thermal properties as well as mechanical properties are required.

Table 1. Material properties.

	Disc	Pad	Piston
Young's modulus (GPa)	110	3	210
Poisson's ratio	0.29	0.3	0.3
Density (kg/m <sup>3</sup> )	7,200	2,252	7,900
Thermal expan. (10 <sup>-5</sup> /°C)	1.05	0.76	2.3
Conductivity (w/m°C)	53	0.68	177
Specific heat (J/kg°C)	642	1,465	875

3.2. Natural Frequency Verification

To verify the reliability of the FE model and the material properties, modal analysis results were compared with modal test results. The modal test configurations of the disc and the pad using an impact hammer are shown in Figure 3. The natural frequency and mode shape of the disc and the pad are shown in Table 2. Both disc and pad almost match the natural frequency in modal test and modal analysis.

3.3. Boundary Condition

The boundary condition of the FE model is shown in Figure 4. The disc is constrained to the rotating center node. The brake pads are allowed to make frictional contact with the disc by providing a translational degree of freedom. The thermal boundary conditions of Equations (2) ~ (5) are applied on each surface. A convection coefficient  $h$  ( $= 8 \text{ W/m}^2\text{C}$ ) using Equation (6) decreases

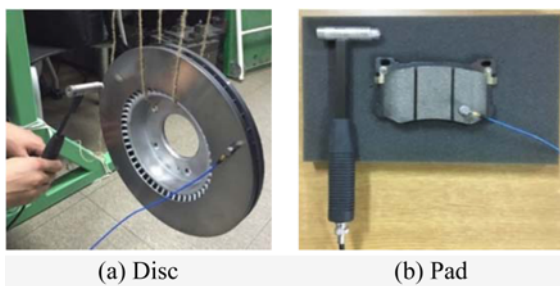
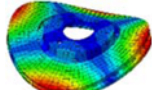
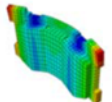


Figure 3. Modal test configuration.

Table 2. Natural frequency and mode shape.

First mode	Test	Analysis		Error (%)
	Freq. (Hz)	Freq. (Hz)	Mode shape	
Disc	1,100	1,112		1.1
Pad	2,200	2,246		2.1

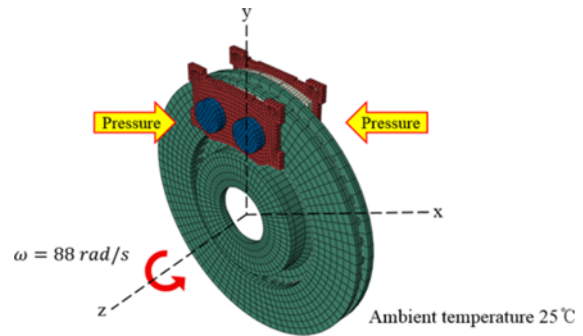


Figure 4. Boundary condition of FE model.

according to disc velocity in Equation (8). A constant braking pressure ( $= 3 \text{ MPa}$ ) decelerates the disc velocity from 88 rad/s to zero. The heat partition ratio  $\gamma$  ( $= 0.91$ ) is obtained from Equation (10). The initial friction coefficient is 0.3 and ambient temperature is 25 °C.

3.4. Temperature Results

From the coupled thermo-mechanical analysis, the temperature results can be confirmed. The temperature distribution on the disc surface is presented in Figure 5. At the initial braking times, it can be seen that the temperature is uniformly distributed. At the end of the braking times, the disc surface formed a thermal band with a local temperature difference.

The temperature results according to different disc radii ( $r = 0.108, 0.124, \text{ and } 0.142 \text{ m}$ ) are shown in Figure 6. During the braking times, the temperature increases steadily and then decreases because of the convective heat transfer at the end of braking.

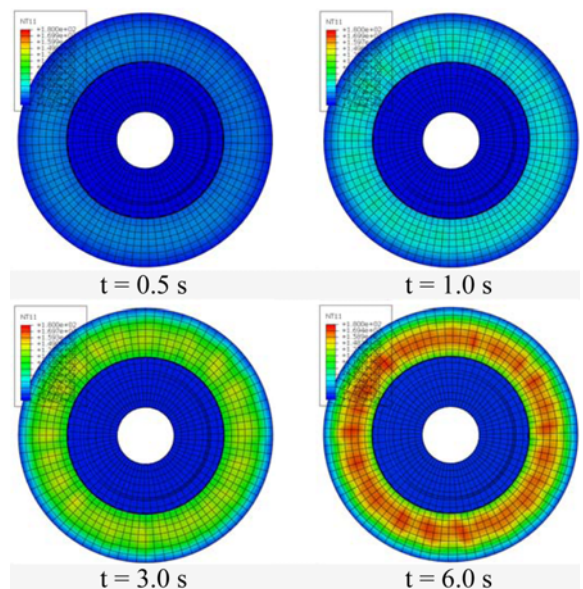


Figure 5. Temperature distribution of the disc surface.

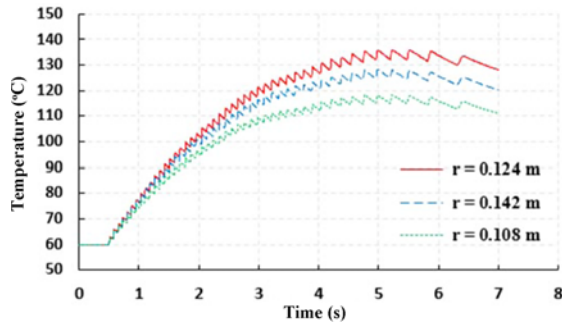


Figure 6. Disc temperature results according to different radii ( $r = 0.108, 0.124,$  and  $0.142$  m).

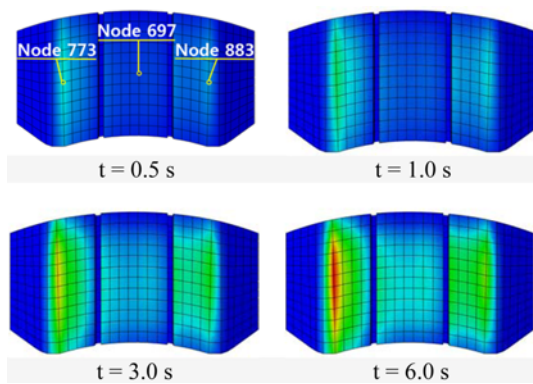


Figure 7. Temperature distribution of the pad surface.

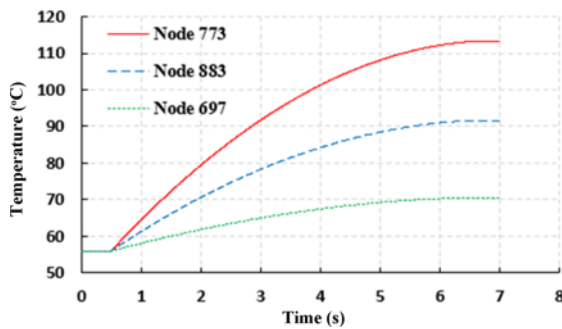


Figure 8. Pad temperature results according to node number (node 773, node 883, and node 697).

The temperature results of the pad surface are presented in Figures 7 and 8. The leading surface node 773, the pad center node 697, and the trailing surface node 883 are shown in Figure 7. The pad temperature increases steadily over the braking times. Because the pad is always in contact with the disc, there is little temperature reduction caused by convective heat transfer.

#### 4. SHAPE OPTIMIZATION

##### 4.1. Description of the Optimization Process

A shape optimization for the non-uniform contact pressure

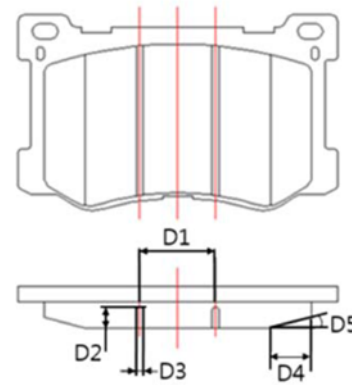


Figure 9. Design parameters of the brake pad.

distribution was carried out to minimize the uneven wear of brake pads. Five parameters that determine the shape of the brake pad are shown in Figure 9. A sensitivity analysis was carried out using a Plackett-Burman design to identify the parameters that have a major effect on the purpose performance (Plackett and Burman, 1946). The parameters  $D_1(=x_1)$  and  $D_4(=x_2)$  are the final design variables. A first-order curve fitting slope value for the dispersed contact pressure values was selected as an indicator of the non-uniform contact pressure distribution.

The minimum (- 1), current (0), and maximum (+ 1) design values according to three-level factor are shown in Table 3. The results of the central composite design are shown in Table 4. The length unit of  $x_1$  and  $x_2$  is mm.

The shape optimization was performed using a response

Table 3. Design parameter level.

Factor	Level		
	Min. (- 1)	Current (0)	Max. (+ 1)
$x_1$	20	30	40
$x_2$	5	16	21

Table 4. Central composite design table.

No.	$x_1$	$x_2$	Result
1	20	5	0.0578
2	20	21	0.1961
3	40	5	0.0587
4	40	21	0.1895
5	30	16	0.1255
6	20	16	0.1167
7	40	16	0.1287
8	30	5	0.0581
9	30	21	0.1808

surface methodology. The second-order regression model function, which is the response surface, can be derived from the central composite design table (Myers and Montgomery, 2002). In this shape optimization, the second-order regression model function is the objective function representing the response surface of the first-order curve fitting slope value for the dispersed contact pressure values. The second-order regression model function is derived as follows:

$$\hat{y} = 0.1215 + 0.0010x_1 + 0.0653x_2 + 0.0031x_1^2 - 0.0001x_2^2 - 0.0019x_1x_2 \quad (13)$$

Moreover, the second-order regression model function is a quadratic programming (QP) problem. The general mathematical equation of a QP problem can be expressed as follows:

$$\hat{y} = x^T Px + x^T q + r \quad (14)$$

where  $\hat{y}$  and  $x$  are the objective function and design variable, respectively.  $P$ ,  $q$ , and  $r$  are the matrix with estimated coefficients of the quadratic, linear, and intercept terms, respectively. The optimum value of QP can be obtained as a zero point by first order differentiation of the objective function for each variable.

$$\frac{\partial \hat{y}}{\partial x} = 2Px + q = 0 \quad (15)$$

$$x_s = -\frac{1}{2}P^{-1}q \quad (16)$$

The QP optimization formula for the non-uniform contact pressure distribution of the brake pad is defined as follows:

$$\begin{aligned} &\text{Min. } x^T Px + x^T q + r \\ &\text{Subject to } -1 < \frac{1}{2}x_1 - x_2 < 5 \end{aligned} \quad (17)$$

The analysis of variance (ANOVA) table that verifies the reliability of the regression model function is shown in Table 5. Because  $F_0 \geq F(0.01)$  in the ANOVA table, the

Table 5. ANOVA table.

Factor	S	$\Phi$	V	F0	F (0.01)
Reg. V	0.0257	2	0.01285	385.5	4.43
Res. V	0.0002	6	0.00003		
Sum	0.0259	8			

Table 6. Optimization results.

Factor	Initial value	Optimum value
$x_1$	30	25
$x_2$	16	11

estimated model is reliable at the significance level of 1 %. Thus, the objective function is well defined.

The optimum design values of  $x_1$  and  $x_2$  that minimize the objective function are shown in Table 6.

4.2. Optimization Results of the Contact Pressure Distribution and Temperature Distribution

The analysis results of the initial and the optimized pads were compared. The analysis results of the contact pressure distribution and temperature distribution are shown in Figures 10 and 11. During all braking times, the contact pressure distribution of the pad is, as expected, concentrated at the leading surface where the friction starts. The maximum contact pressure of the initial pad is 4.24 MPa, while the maximum contact pressure of the optimized pad is 3.61 MPa. Therefore, the maximum contact pressure of the optimized pad is reduced by about 15.0 % compared to that of the initial pad.

The temperature distribution of the pad is concentrated at the leading surface. The maximum temperature of the initial pad is 113 °C, while the maximum temperature of the optimized pad is 104 °C. Therefore, the maximum temperature of the optimized pad is reduced by about 8.0 % compared to that of the initial pad.

The objective function results of the initial and optimized pads are shown in Figures 12 and 13. Because of the geometry change, the mesh node of the optimized pad is increased by two compared to that of the initial pad. The objective function is reduced by about 26.1 %, from 0.1487 in the initial pad to 0.11 in the optimized pad. Therefore, the non-uniform contact pressure distribution is clearly reduced with the shape optimization.

The first-order curve fitting slope value at the optimum

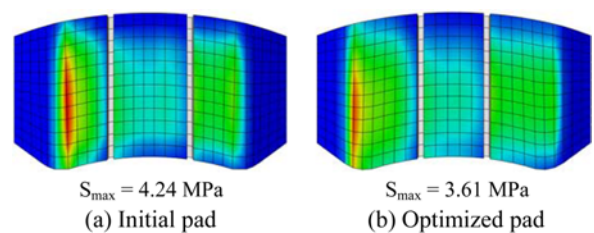


Figure 10. Contact pressure distribution of the initial and optimized pads.

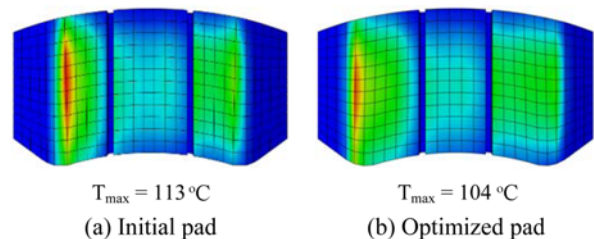


Figure 11. Temperature distribution of the initial and optimized pads.

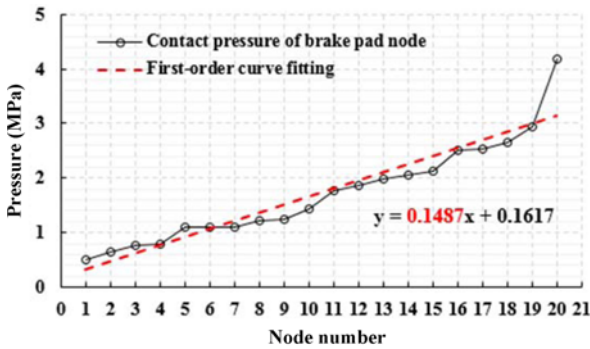


Figure 12. First-order curve fitting slope value for the dispersed contact pressure values of the initial pad.

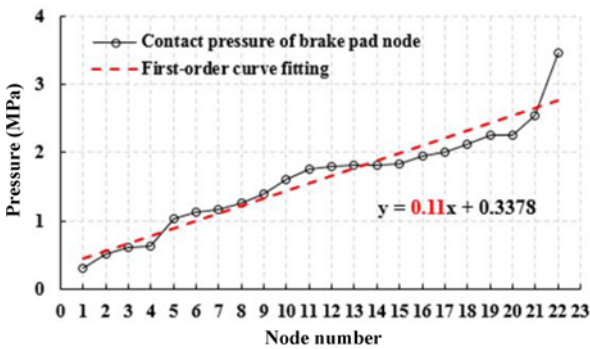


Figure 13. First-order curve fitting slope value for the dispersed contact pressure values of the optimized pad.

value can be obtained using the derived second-order regression model function. The optimum values  $x_1$  and  $x_2$  are the actual unit values resulting from the optimization. Therefore, by converting these values back to the coded values and substituting those into the second-order regression model function, which is an objective function, the first-order curve fitting slope value can be easily obtained. The coded value  $X_i$  corresponding to actual unit value  $x_i$  can be defined as

$$x_i = \frac{X_i - [\max(x_i) + \min(x_i)]/2}{[\max(x_i) - \min(x_i)]/2} \quad (i = 1, 2) \quad (18)$$

The comparison results for the first-order curve fitting slope value of the contact pressure between the analysis and the objective function are shown in Table 7. The results obtained by using the analysis and the objective function are almost the same. Therefore, the effect of the non-

Table 7. First-order curve fitting slope value of the contact pressure between analysis and objective function.

	Initial pad	Optimized pad
Analysis	0.1487	0.1100
Objective function	0.1460	0.1052

uniform contact pressure distribution can be easily found using the objective function without analysis.

## 5. BRAKE DYNAMOMETER TEST

### 5.1. Description of Test Environment

A brake dynamometer test was conducted to measure the amount of pad wear. The configuration of the brake dynamometer test is shown in Figure 14. The brake disc is connected to the brake dynamometer rotating part. A thermocouple sensor is connected to the disc outboard surface and the pad friction surface. The disc is equipped with brake caliper and pads.

The performance test of the brake pad was carried out using the JASO C406\_2000 (2016) test specification. The first fade mode in the JASO C406\_2000 test specification was used as the experimental result. The first fade mode can test the brake pad performance with rapid braking conditions from an initial speed of about 100 km/h.

### 5.2. Temperature Result Comparison

The analysis temperatures of the brake disc and the pad were compared with the experimental temperatures. The thermocouple configuration for measuring the temperature at the disc surface and at the center of the pad surface is shown in Figure 15.

The temperature results of the disc and the pad in the brake dynamometer test and the FE analysis are shown in Figures 16 and 17. The initial temperature before braking is constant at about 60 and 56 °C, respectively. The temperature rises slightly from 0.5 sec after braking starts.

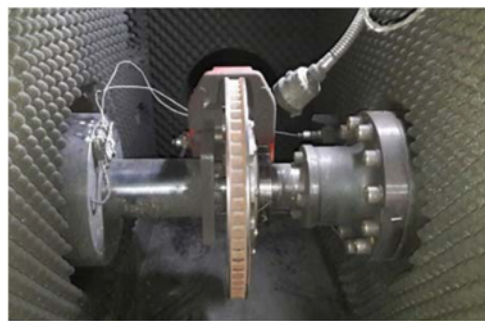


Figure 14. Configuration of brake dynamometer test.

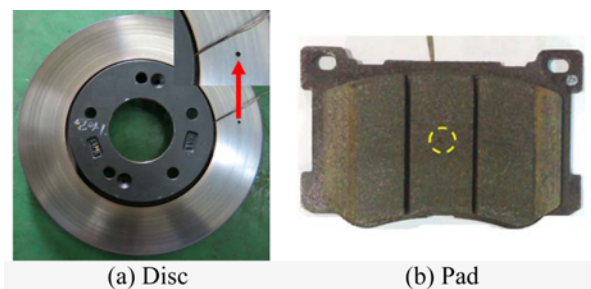


Figure 15. Thermocouple in disc and pad.

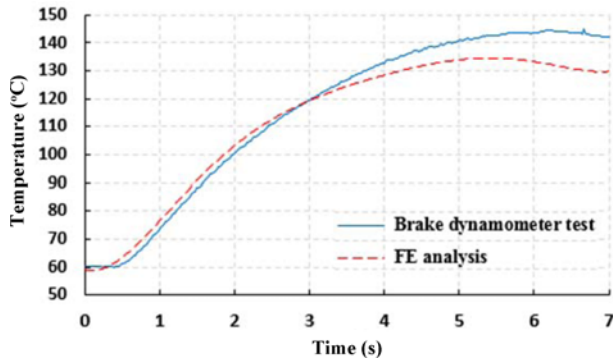


Figure 16. Temperature at the friction surface of the disc.

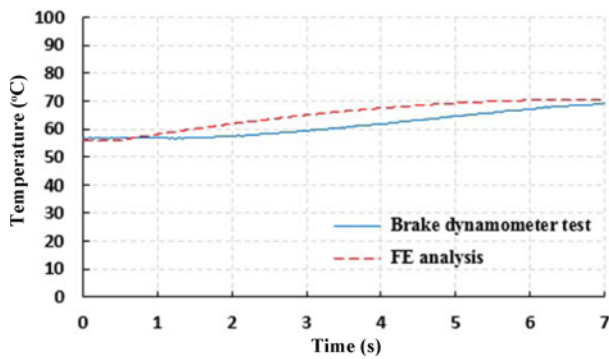


Figure 17. Temperature at the center of the pad.

At the end of braking, the analysis temperature of the disc is about 130 °C, with a difference of only about 8.1 % with the test. On the other hand, the analysis temperature of the pad is about 70 °C, with a difference of only about 1.9 % with the test. Considering the nonlinear material properties of the disc and pad, the boundary conditions, and the errors of the experiment and analysis, the analysis temperatures for the disc and the pad approximately correspond to the experimental results.

5.3. Wear Test Result

Eight check-points were selected to measure the amount of wear in the brake pad, as shown in Figure 18. The check-

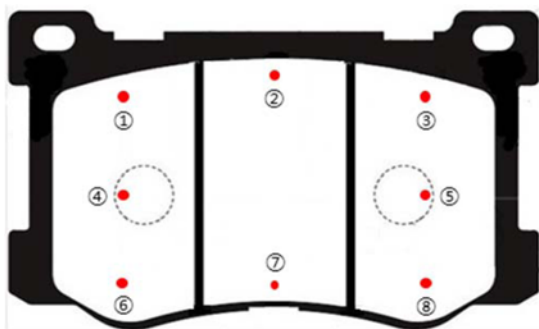


Figure 18. Check-points on the brake pad surface.

Table 8. Height results of the brake pad. (unit: mm)

Check point	Initial pad		Optimized pad	
	Before	After	Before	After
①	16.36	16.14	16.39	16.21
②	16.32	16.24	16.34	16.29
③	16.40	16.28	16.40	16.30
④	16.38	16.03	16.42	16.15
⑤	16.39	16.21	16.45	16.24
⑥	16.35	16.07	16.42	16.19
⑦	16.38	16.27	16.47	16.33
⑧	16.39	16.26	16.46	16.29

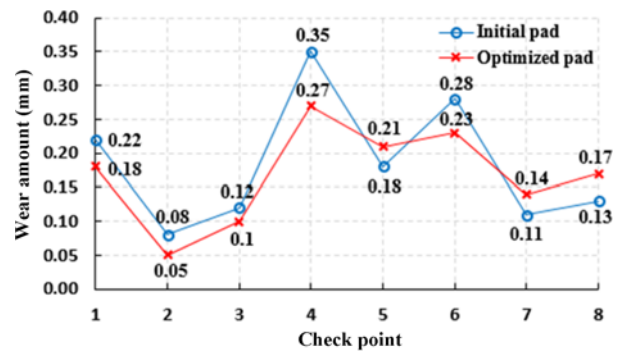


Figure 19. Wear amount of the brake pad at check-points.

point at the center of the brake pad was excluded because the pad temperature had to be measured by inserting a thermocouple sensor. The check-points at the leading surface are ①, ④ and ⑥.

The results of measuring the height of the brake pad wear, before and after the brake dynamometer test, are shown in Table 8. The height of the brake pad wear was measured using a digital height gauge (Mitutoyo Digital Height Gauge 192-613).

The difference in wear amount at the check-points for the initial and the optimized pads is shown in Figure 19. The wear amount of the optimized pad was much lower than that of the initial pad. In particular, the wear amount in check-points ①, ④, and ⑥, where the contact pressure distribution is concentrated, was greatly reduced. On the contrary, there are points where the amount of wear is increased. However, because the standard deviation of the amount of wear was reduced from the viewpoint of the pad's uneven wear, it can be concluded that the uneven wear of the optimized pad is reduced compared to the initial pad.

The standard deviation of the wear amount of the initial and optimized pads is shown in Table 9. The standard deviation of the optimized pad was reduced by about 24.0 % compared to the initial pad.



Table 9. Standard deviation of the wear amount.

	Initial pad	Optimized pad
Standard deviation	0.09365	0.07120
Reduction percent	24.0 %	

## 6. CONCLUSION

Non-uniform contact pressure distribution is a major cause of uneven wear in brake pads. In this paper, a coupled thermo-mechanical analysis was carried out to confirm the non-uniform contact pressure distribution of the disc and pad. The contact pressure and temperature were higher at the leading surface, where friction starts. The analysis and experimental temperature results for the disc and the pad were almost the same. The wear amount of the brake pad was measured through a brake dynamometer test to confirm the correlation between the non-uniform contact pressure distribution and uneven wear. Experimental results show that wear occurs more in the leading surface than in the trailing surface. In addition, a shape optimization for reducing the uneven wear was conducted. The second-order regression model function can be used to predict the effect of the non-uniform contact pressure. Moreover, the second-order regression model function can be used to easily compare uneven wear if only design variable values are given. As a result of the optimization, the uneven wear of the brake pad was reduced by about 24.0 %.

**ACKNOWLEDGEMENT**—This research was financially supported by Jeollanamdo Province and Jeonnam Institute for Regional Program Evaluation (JNIRPE) through the Research and Development for Auto Tuning Part Industry, “Developed high-performance tuning brake friction material with improved fade resistance and durability life by using composite materials (B0080530000117)”.

## REFERENCES

- Abubakar, A. R. and Ouyang, H. (2008). Wear prediction of friction material and brake squeal using the finite element method. *Wear* **264**, **11**, 1069–1076.
- Baillet, L., Linck, V., D’Errico, S., Laulagnet, B. and Berthier, Y. (2005). Finite element simulation of dynamic instabilities in frictional sliding contact. *J. Tribology* **127**, **3**, 625–657.
- Frank, P. I., David, P. D., Theodore, L. B. and Adrienne, S. L. (2013). *Foundations of Heat Transfer*. 6th edn. John Wiley & Sons. New York, USA.
- Gao, C. H., Huang, J. M., Lin, X. Z. and Tang, X. S. (2006). Stress analysis of thermal fatigue fracture of brake disks based on thermomechanical coupling. *J. Tribology* **129**, **3**, 536–543.
- Hassan, M. Z., Brooks, P. C. and Barton, D. C. (2009). A predictive tool to evaluate disk brake squeal using a fully coupled thermo-mechanical finite element model. *Int. J. Vehicle Design* **51**, **1-2**, 124–142.
- JASO C406\_2000 (2016). <http://wenku.baidu.com/view/116fd41dfad6195f312ba69e.html>
- Jung, S. P., Park, T. W., Chai, J. B. and Chung, W. S. (2011). Thermo-mechanical finite element analysis of hot judder phenomenon of a ventilated disc brake system. *Int. J. Precision Engineering and Manufacturing* **12**, **5**, 821–828.
- Lee, K. J. and Barber, J. R. (1994). An experimental investigation of frictionally-excited thermoelastic instability in automotive disk brakes under a drag brake application. *J. Tribology* **116**, **3**, 409–414.
- Limpert, R. (1999). *Brake Design and Safety*. 2nd edn. SAE International. Warrendale, Pennsylvania, USA.
- Meziane, A., D’Errico, S., Baillet, L. and Laulagnet, B. (2007). Instabilities generated by friction in a pad-disc system during the braking process. *Tribology Int.* **40**, **7**, 1127–1134.
- Myers, R. H. and Montgomery, D. C. (2002). *Response Surface Methodology*. 2nd edn. John Wiley & Sons. New York, USA.
- Pantuso, D., Bathe, K. J. and Bouzinov, P. A. (2000). A finite procedure for the analysis of thermal-mechanical solids in contact. *Computers & Structures* **75**, **6**, 551–573.
- Parker, R. C. and Marshall, P. R. (1948). The measurement of the temperature of sliding surfaces with particular reference to railway blocks. *Proc. Institute of Mechanical Engineers* **158**, **1**, 209–229.
- Plackett, R. and Burman, J. (1946). The design of optimum multifactorial experiments. *Biometrika* **33**, **4**, 305–325.
- Söderberg, A. and Andersson, S. (2009). Simulation of wear and contact pressure distribution at the pad-to-rotor interface in a disc brake using general purpose finite element analysis software. *Wear* **267**, **12**, 2243–2251.
- Thomas, J. M., Steven, C. N. et al. (2002). Thermal cracking in disc brakes. *Engineering Failure Analysis* **9**, **1**, 63–76.
- Wu, S. C., Zhang, S. Q. and Xu, Z. W. (2016). Thermal crack growth-based fatigue life prediction due to braking for a high-speed railway brake disc. *Int. J. Fatigue*, **87**, 359–369.
- Yevtushenko, A. and Grzes, P. (2011). Finite element analysis of heat partition in a pad/disc brake system. *Numerical Heat Transfer* **59**, **7**, 521–542.